J Mol Model (2013) 19:5355–5365
DOI 10.1007/s00894-013-2029-z

ORIGINAL PAPER

A DFT study on the thermal cracking of JP-10

Lei Yue · Hu-Jun Xie · Xiao-Mei Qin · Xiao-Xing Lu · Wen-Jun Fang

Received: 3 August 2013 / Accepted: 7 October 2013 / Published online: 27 October 2013

Abstract Density functional theory (DFT) calculations have been carried out to investigate the thermal cracking pathways of JP-10, a high energy density hydrocarbon fuel. Thermal cracking mechanisms are proposed, as supported by our previous experimental results (Xing et al. in Ind Eng Chem Res 47:10034–10040, 2008). Using DFT calculations, the potential energy profiles of the possible thermal cracking pathways for all of the diradicals obtained from homolytic C–C bond cleavage of JP-10 were derived and are presented here. The products of the different thermal cracking pathways are in good agreement with our previous experimental observations.

Keywords DFT calculations · JP-10 · Thermal cracking · Reaction mechanism

Introduction

JP-10 (*exo*-tetrahydrodicyclopentadiene, $C_{10}H_{16}$) is a popular missile fuel, and it is also used in volume-limited combustion applications such as in ramjets and scramjets, due to its high energy density, high heat capacity, low freezing point, and favorable handling characteristics. Although studies [1–11] have been conducted to investigate the physical properties and catalytic cracking of JP-10 at various temperatures and pressures by means of spectroscopic, gas chromatographic, and mass spectrometric analyses, the high-temperature thermal decomposition chemistry of JP-10 is still not well understood.

Our group [12–19] has performed fundamental research on the thermal oxidation stability, physical properties, and catalytic cracking of JP-10 under different conditions. The experimental results we obtained indicate that the predominant hydrocarbon products of catalytic cracking are methane, ethane, ethene, propane, and propylene in the gaseous phase, and benzene, indene, naphthalene, and their homologs in the liquid phase. The thermal decomposition of JP-10 also yields diverse products [5, 8, 20–24]. The variation in experimental conditions may provide some explanation for the diversity of the observed products.

Goddard et al. [25] have carried out molecular dynamic simulations employing the ReaxFF reactive force field to investigate the thermal oxidation and decomposition reactions of JP-10. Their results show that the thermal decomposition of JP-10 is initiated by C–C bond cleavage, resulting in either the production of ethylene plus a C_8 hydrocarbon or two C_5 hydrocarbons. The temperature dependence of the product distribution between C_1 and C_5 was derived and found to be in good agreement with experimental observations. Jaffe et al. [26] have performed high-level ab initio calculations to study the *exo* and *endo* isomers of gas-phase tetrahydrodicyclopentadiene (THDCPD). The calculated values for the gas-phase heat of formation of $\Delta_f H°(298)$ are −126.4 and −114.7 kJ mol^{-1} for the *exo* and *endo* isomers, respectively. These results suggest that the isodesmic bond separation reaction, $C_{10}H_{16} + 14CH_4 \rightarrow 12C_2H_6$, can explain the production of the *exo* isomer (JP-10). Williams et al. [27] have investigated the ignition of JP-10 by means of theoretical methods. They showed that the chemical mechanism of ignition consists of 174 elementary steps involving 36 chemical species. The ignition times predicted by the new detailed mechanism were found to be in good agreement

L. Yue · H.-J. Xie · X.-M. Qin · X.-X. Lu · W.-J. Fang (✉)
Department of Chemistry, Zhejiang University, Hangzhou 310027, China
e-mail: fwjun@zju.edu.cn

H.-J. Xie (✉)
Department of Applied Chemistry, Zhejiang Gongshang Universty, Hangzhou 310035, China
e-mail: hujunxie@gmail.com

with data from JP-10 shock-tube experiments. Bozzelli et al. [28] have reported the thermochemical properties of JP-10. The standard enthalpy of formation of JP-10 and different tricyclodecyl radicals corresponding to the loss of H atoms from the carbon sites were evaluated using five density functional methods along with the G3MP2B3 and CBS-QB3 composite computational methods. Five isodesmic reactions that included reference molecules with similar ring strains were used in order to cancel out calculation errors.

Our group [29] has investigated the thermal cracking of JP-10 in a batch reactor under different pressures. The gaseous and liquid components were determined quantitatively by gas chromatography and gas chromatography–mass spectrometry, respectively. A possible mechanism for the thermal cracking of JP-10 that could explain the product distribution was proposed. In the work described in the present paper, density functional theory (DFT) calculations were performed to study the thermal decomposition chemistry of JP-10 in detail.

Computational details

All geometries of the reactants, intermediates, transition states, and products involved in the thermal cracking reactions of JP-10 were fully optimized by means of DFT calculations using the M06-2X functional [30, 31]. The reliability of the chosen method has already been demonstrated by various work [32–37]. The 6-31+g(d) basis set was used for the C, O, and H atoms. Frequency analyses were performed to obtain the zero-point energies (ZPE) and identify all of the stationary points as minima (no imaginary frequency) or transition states (one imaginary frequency) on the potential energy surfaces (PES). Intrinsic reaction coordinate (IRC) calculations were also performed for the transition states to confirm that these structures do indeed connect two relevant minima [38, 39]. All calculations were performed with the Gaussian09 software package [40].

Results and discussion

Figure 1 describes the possible biradicals obtained from the homolytic C–C bond cleavage of JP-10. Table 1 gives the relative energies (REs) of the seven possible biradicals of JP-10 shown in Fig. 1. It should be noted that biradical **R_1** involving C1–C2 bond cleavage is the most stable species, while biradical **R_7** involving C3–C4 bond cleavage is the least stable species, and is higher in energy than **R_1** by 10.1 kcal mol^{-1}. The calculated relative energies of biradicals **R_2** and **R_3** are similar, while **R_3** is slightly more stable than **R_2** by 0.3 kcal mol^{-1}. The biradical can then abstract one hydrogen atom from a JP-10 molecule to yield a variety of radicals, as presented in Fig. 2, where the relative energies are shown in parentheses. According to the DFT calculations, the radical **3_8** is the most stable species and the radical **5_4** is the most unstable species. Thus, we take the energy of radical **3_8** as zero in the following calculations.

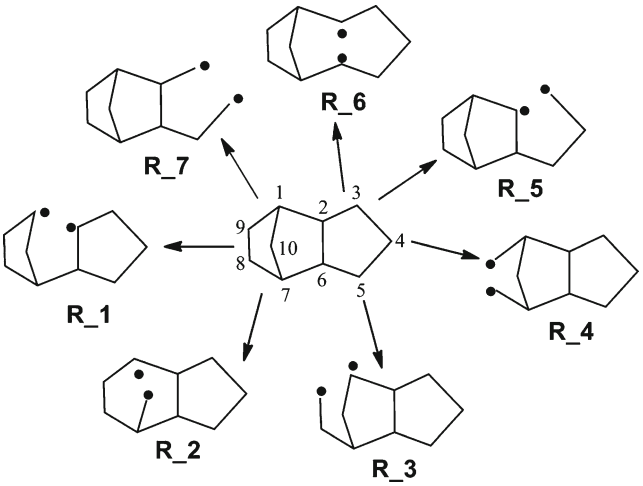

Fig. 1 Possible biradicals result from the homolytic C–C bond cleavage of JP-10

Possible thermal cracking pathways for diradical R_1

We first consider the possible thermal cracking pathways of diradical **R-1** of JP-10. **R-1** can abstract one hydrogen atom from another JP-10 to form radical **1_1** or radical **1_3**. Figure 3 shows the two possible thermal cracking pathways of diradical **R-1** of JP-10. Path **a** is a direct C–C bond dissociation that yields a cyclopentane radical and cyclopentene, and the former active compound can then convert into the cyclopentane. Path **b** (paths **bi**/**bii**) considers the consequences of breaking the five-membered ring during the thermal cracking pathway. The free-energy profiles for thermal cracking paths **a** and **b** of diradical **R-1** are displayed in Fig. 4.

In path **a** (Fig. 4), starting from the radical **1_1**, the C6–C7 bond is directly dissociated via the transition state $\mathbf{TS_1}$ to give a cyclopentane radical and cyclopentene. This result is consistent with our experimental observations that cyclopentane and cyclopentene are found in the product component analysis [29].

Table 1 The relative energies (REs, in kcal mol^{-1}) of the seven possible diradicals of JP-10 shown in Fig. 1

Species	RE (kcal mol^{-1})
R_1	0.0
R_2	2.8
R_3	2.5
R_4	8.0
R_5	9.7
R_6	4.2
R_7	10.1

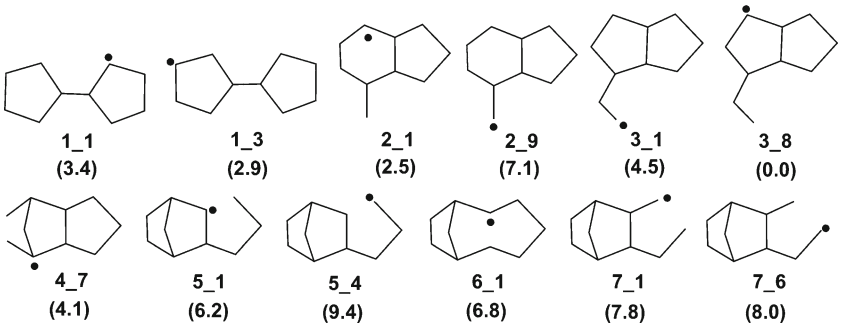

Fig. 2 Possible radicals derived from the homolytic C–C bond cleavage of JP-10 followed by the abstraction of one hydrogen atom from a new JP-10 molecule. The relative free energies (kcal mol^{-1}) are shown in *parentheses*

The barrier ($\mathbf{TS_1}$) to C–C bond cleavage is calculated to be 25.6 kcal mol^{-1}, and the C–C distance in $\mathbf{TS_1}$ is equal to 2.244 Å.

Path **b** has two possibilities (path **bi** and path **bii**) for the thermal cracking of diradical **R-1**. In path **bi** (Fig. 4), the C7–C10 bond is cleaved in radical **1_3** to produce radical **1_4** via the transition state $\mathbf{TS_2}$, and the barrier is 32.4 kcal mol^{-1}. This step is endergonic by 16.4 kcal mol^{-1}. From **1_4**, there are two possible pathways for the thermal cracking reaction. It is found that the pathway involving C8–C9 bond cleavage is kinetically more favorable, and this has a barrier ($\mathbf{TS_3}$) of 21.1 kcal mol^{-1} from **1_4** to $\mathbf{TS_3}$. The overall barrier from **1_3** to $\mathbf{TS_3}$ is about 37.5 kcal mol^{-1}. In path **bii** (Fig. 4), the C8–C9 bond is cleaved in compound **1_3**, which is followed by C7–C10 bond cleavage to give the final products (Fig. 4: **1_3** → $\mathbf{TS_6}$ → **1_6** → $\mathbf{TS_7}$ → **1_5**). The overall barrier for this path from **1_3** to $\mathbf{TS_7}$ is calculated to be 39.5 kcal mol^{-1}.

According to the calculations, thermal cracking path **a** of diradical **R-1** is kinetically more favorable than paths **bi** and **bii**, with a barrier of only 25.6 kcal mol^{-1}.

Possible thermal cracking pathways for diradical R_2

Starting from **R_2**, two thermal cracking pathways (paths **c** and **d**) are possible. Figure 5 presents the possible thermal cracking pathways of diradical **R-2** of JP-10, and the calculated free-energy profiles are displayed in Fig. 6.

From Fig. 6, it is clear that path **d** is kinetically more favorable. In path **d** (Fig. 6), the hydrogen atom in **2_9** is transferred from the C7 atom to the C10 atom via **TS** to generate the C7-centered radical **2_6**, and the barrier is about 35.1 kcal mol^{-1}. Then the C5–C6 bond is dissociated to give the C5-centered radical **2_7**, with a predicted barrier ($\mathbf{TS_4}$) of 23.5 kcal mol^{-1}. From **2_7**, another hydrogen atom transfer takes place to form the C4-centered radical **2_8**, with a barrier of 37.5 kcal mol^{-1}. Finally, the C2–C3 bond breaks to give propene and radical **2_4**, and the latter radical can further form toluene, which has been found in the experimental products [29]. For path **d**, the overall barrier from **2_6** to $\mathbf{TS_5}$ is predicted to be 52.9 kcal mol^{-1}.

Possible thermal cracking pathways for diradical R_3

We consider the possible thermal cracking pathways of diradical **R-3** of JP-10 in Fig. 7. The free-energy profiles for thermal cracking paths **e** and **f** of diradical **R-3** of JP-10 are displayed in Fig. 8.

According to the calculations, path **f** is kinetically more favorable than path **e**. In path **f**, the C2–C3 bond in radical **3_8** dissociates via $\mathbf{TS_1}$ to give **3_9**, and the barrier is calculated to be 26.7 kcal mol^{-1}. From **3_9**, the hydrogen atom is transferred from the C4 atom to the C3 atom, followed by C2–C3 bond cleavage. The overall barrier from **3_8** to $\mathbf{TS_2}$ for path **f** is calculated to be 56.1 kcal mol^{-1}.

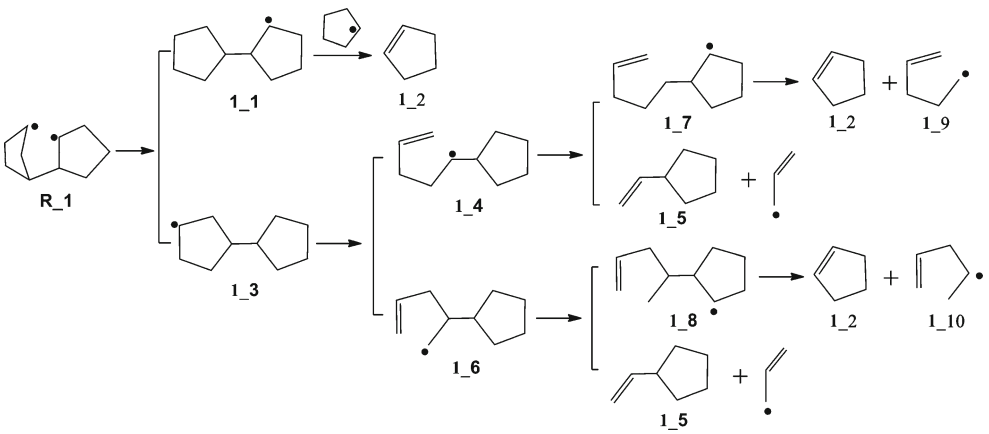

Fig. 3 Possible thermal cracking pathways of diradical **R-1** of JP-10

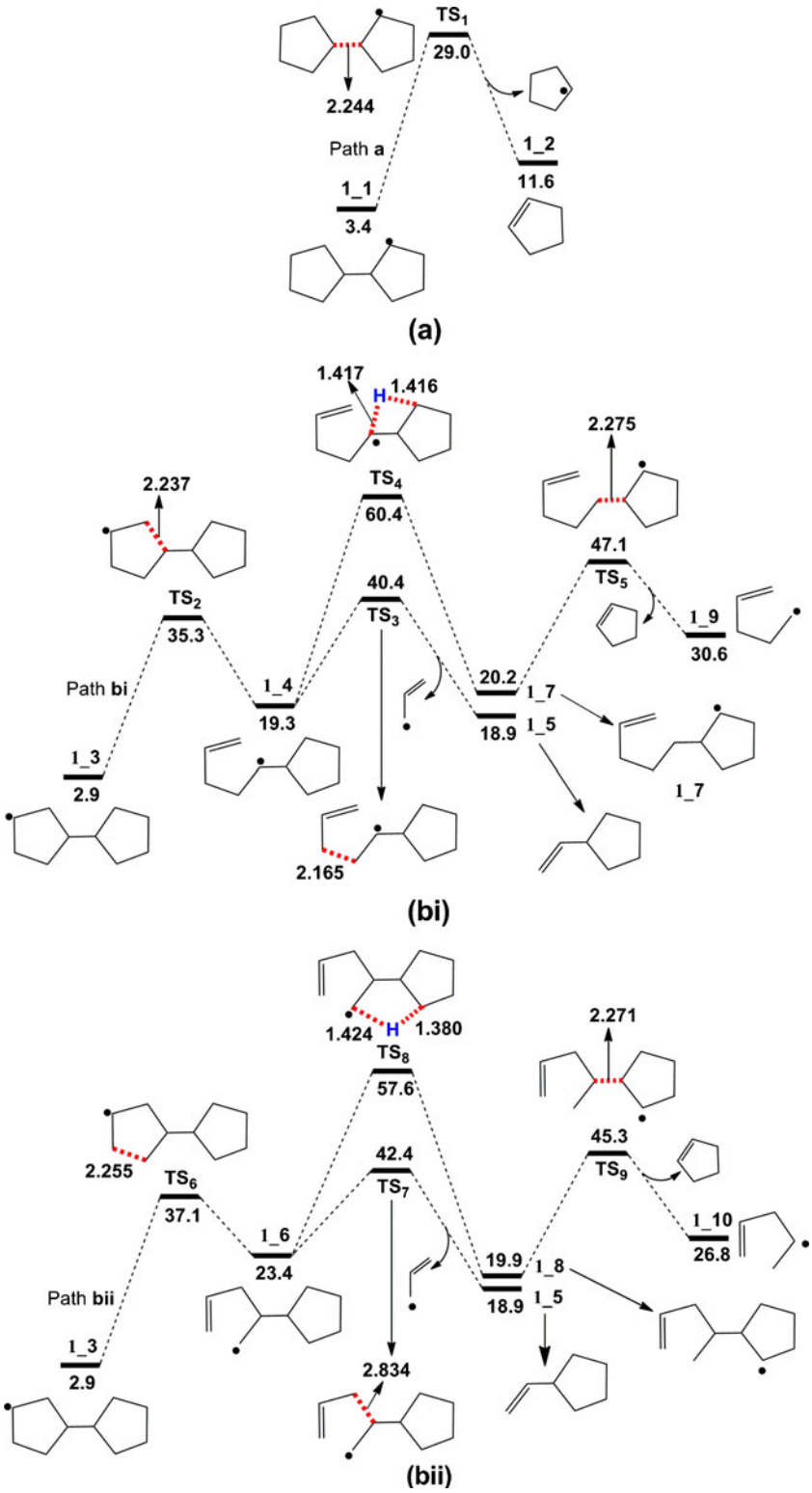

Fig. 4 The free-energy profiles for thermal cracking paths **a** and **b** (**bi**/**bii**) of diradical **R-1** of JP-10. The relative free energies are given in kcal mol^{-1}, and the bond lengths are given in angstroms (Å)

Possible thermal cracking pathway for diradical R_4

Figure 9 shows the possible thermal cracking pathway of diradical **R-4** of JP-10, and the corresponding free-energy profile is displayed in Fig. 10.

In **4_7**, the hydrogen atom is transferred from the C7 atom to the C8 atom to give the C7-centered radical **4_1**. The barrier (**TS**) for hydrogen atom transfer is about 35.6 kcal mol^{-1}. In **4_1**, the C5–C6 bond breaks and a second hydrogen atom is transferred from the C4 atom to the C5 atom

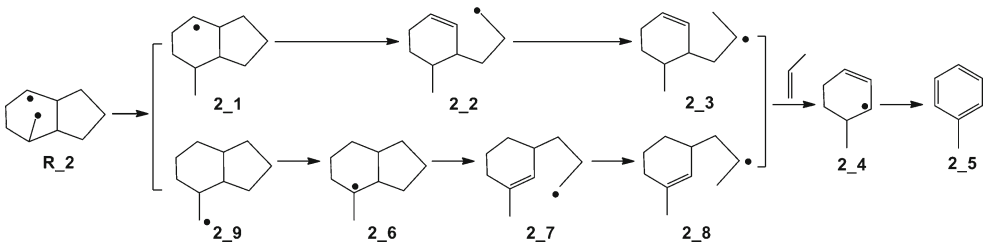

Fig. 5 Possible thermal cracking pathways of diradical **R-2** of JP-10

to form **4_3**. The overall barrier from **4_1** to $\mathbf{TS_2}$ is calculated to be 56.5 kcal mol^{-1}. Then a third hydrogen atom transfer takes place, followed by C9–C1 bond dissociation, to yield 1-methylcyclopentadiene (**4_5**), which was found in experimental products [29].

Possible thermal cracking pathways for diradical R_5

Figure 11 depicts two possible thermal cracking pathways of diradical **R-5** of JP-10, and the free-energy profiles for paths **g** and **h** are presented in Fig. 12.

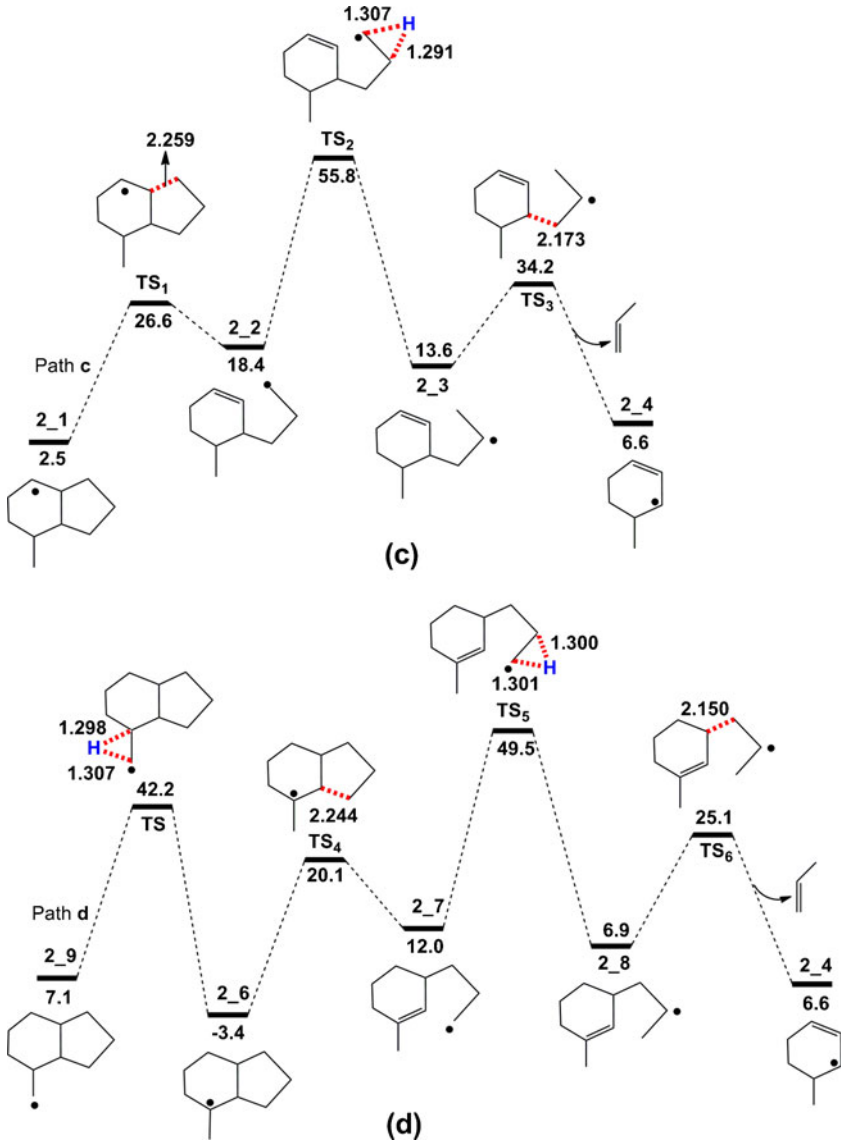

Fig. 6 The free-energy profiles for thermal cracking paths **c** and **d** of diradical **R-2** of JP-10. The relative free energies are given in kcal mol^{-1}, and the bond lengths are given in angstroms (Å)

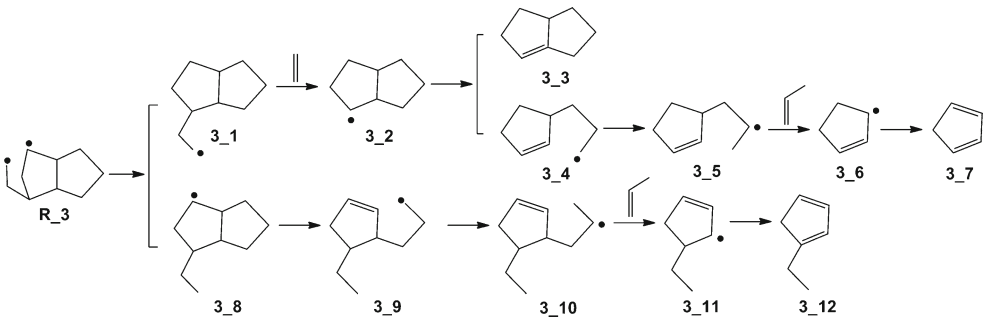

Fig. 7 Possible thermal cracking pathways of diradical **R-3** of JP-10

According to the calculations, path **h** is kinetically more favorable than path **g**. In path **h**, the hydrogen atom in radical **5_4** is transferred from the C4 atom to the C3 atom to form the C4-centered radical **5_5**. The barrier ($\mathbf{TS_1}$) is predicted to be

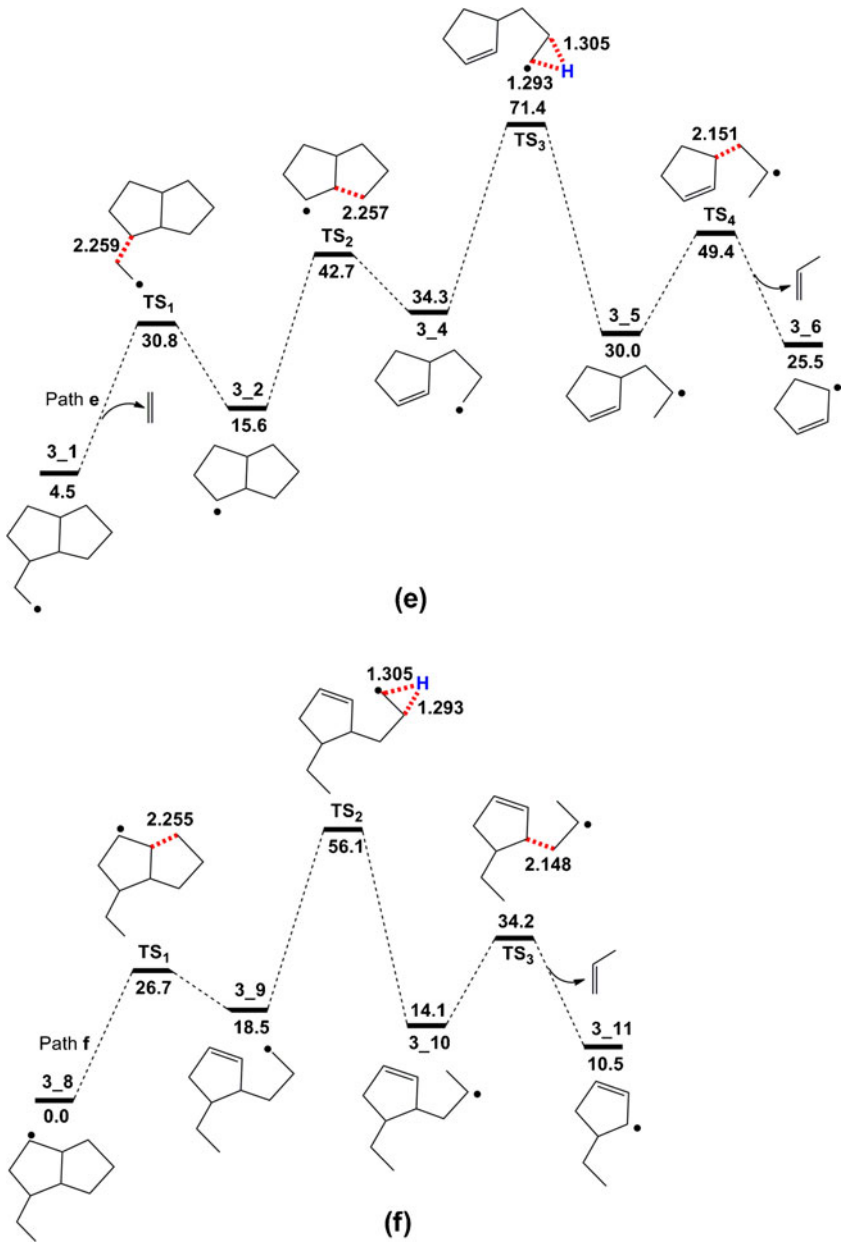

Fig. 8 The free-energy profiles for thermal cracking paths **e** and **f** of diradical **R-3** of JP-10. The relative free energies are given in kcal mol^{-1}, and the bond lengths are given in angstroms (Å)

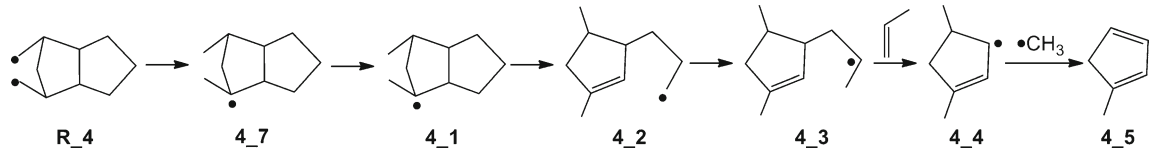

Fig. 9 Possible thermal cracking pathway of diradical **R-4** of JP-10

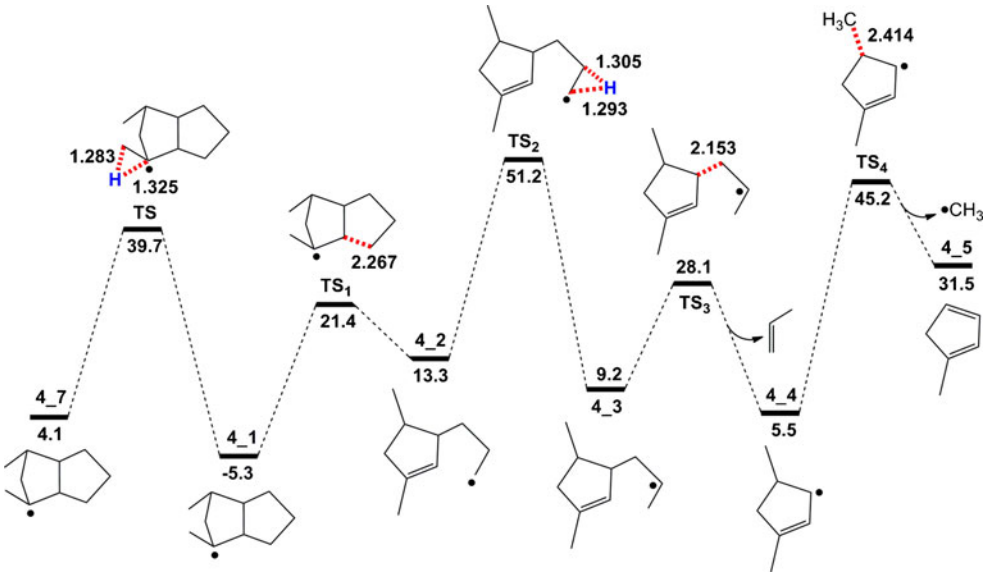

Fig. 10 The free-energy profile for the thermal cracking path of diradical **R-4** of JP-10. The relative free energies are given in kcal mol^{-1}, and the bond lengths are given in angstroms (Å)

37.7 kcal mol^{-1}. In **5_5**, the C5–C6 bond breaks and C7–C10 bond dissociation then occurs, resulting in the radical **5_7**. A second hydrogen atom transfer occurs to give **5_8**, which can finally form the toluene found in the thermal cracking experiments [29]. The overall barrier from **5_5** to **TS$_4$** is calculated to be 57.2 kcal mol^{-1}, slightly lower than that of path **g** (61.8 kcal mol^{-1} from **5_1** to **TS$_2$**).

Possible thermal cracking pathway for diradical R_6

Figure 13 displays the possible thermal cracking pathway of diradical **R-6** of JP-10, and the free-energy profile is displayed in Fig. 14.

In **6_1**, the C3–C4 bond dissociates to form **6_2**. The barrier (**TS$_1$**) is equal to 28.7 kcal mol^{-1}. In **6_2**, the C5–C6 bond breaks to produce ethane and radical **6_3**. The barrier (**TS$_2$**) for this is calculated to be 24.9 kcal mol^{-1}. According to the calculations, the overall barrier from **6_1** to **TS$_2$** is predicted to be 39.0 kcal mol^{-1}.

Possible thermal cracking pathways for diradical R_7

Figure 15 presents the possible thermal cracking pathways (path **i** and paths **ji**/**jii**) of diradical **R-7** of JP-10, and the free-energy profiles for paths **i** and **j** are shown in Fig. 16.

According to the calculations, path **jii** is kinetically more favorable than path **i** or **ji**. As shown in Fig. 16, the radical **7_5** initially converts into **7_6** via C5–C6 bond dissociation. The barrier (**TS$_1$**) to C–C bond cleavage is calculated to be 27.4 kcal mol^{-1}. In **7_6**, the C7–C10 bond breaks, and then

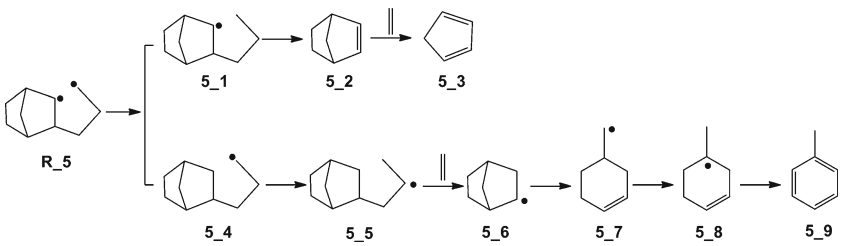

Fig. 11 Possible thermal cracking pathways of diradical **R-5** of JP-10

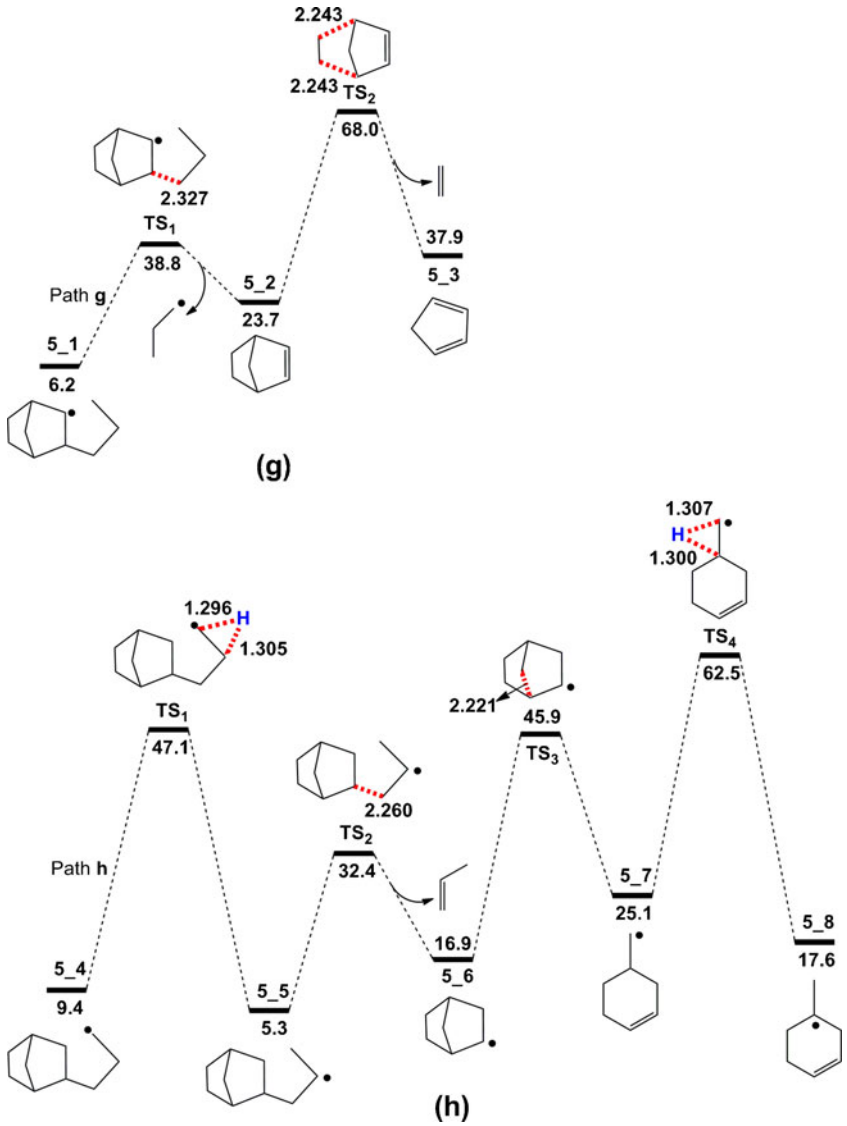

Fig. 12 The free-energy profiles for thermal cracking paths **g** and **h** of diradical **R-5** of JP-10. The relative free energies are given in kcal mol^{-1}, and the bond lengths are given in angstroms (Å)

hydrogen atom transfer occurs to yield radical **7_10**. The overall barrierfrom **7_5** to $\mathbf{TS_5}$ is calculated to be 58.0 kcal mol^{-1}. Finally, C2–C3 bond cleavage takes place to form 1-methylcyclohexadiene **7_11**.

Comparison of the thermal cracking paths for the seven possible diradicals of JP-10

The thermal cracking paths for the seven possible diradicals of JP-10 are now compared. For diradical **R-1**, path **a** (involving the formation of cyclopentane and cyclopentene) is energetically favorable, with a barrier of 25.6 kcal mol^{-1}.

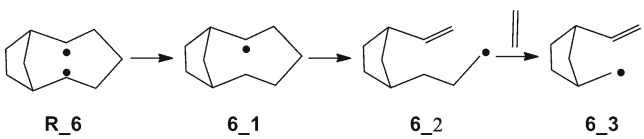

Fig. 13 Possible thermal cracking pathway of diradical **R-6** of JP-10

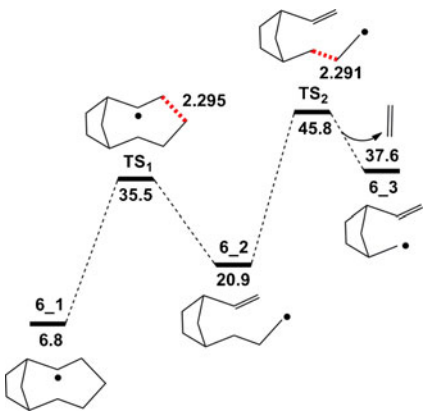

Fig. 14 The free-energy profile for the thermal cracking pathway of diradical **R-6** of JP-10. The relative free energies are given in kcal mol^{-1}, and the bond lengths are given in angstroms (Å)

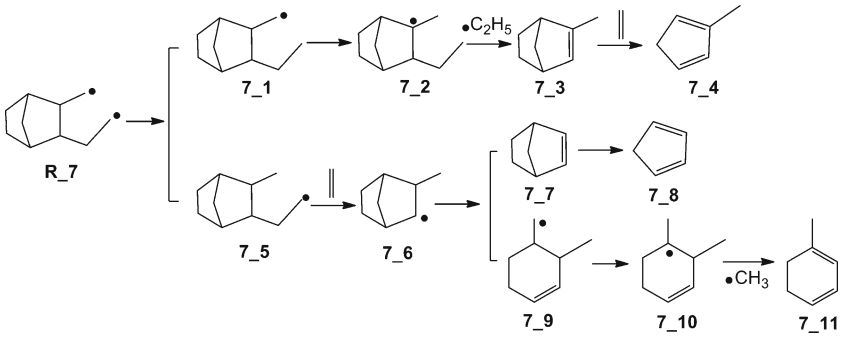

Fig. 15 Possible thermal cracking pathways of diradical **R-7** of JP-10

For diradical **R-2**, path **d** is energetically favorable. From radical **2_9**, a hydrogen atom is transferred and then C5–C6 bond dissociation occurs. Subsequently, another hydrogen atom is transferred, which is accompanied by C2–C3 bond cleavage to give propene and radical **2_4**. The latter radical can then form toluene. The overall barrier from **2_6** to $\mathbf{TS_5}$ is calculated to be 52.9 kcal mol^{-1}. For diradical **R-3**, it is found that path **f** is energetically favorable. In radical **3_8**, the

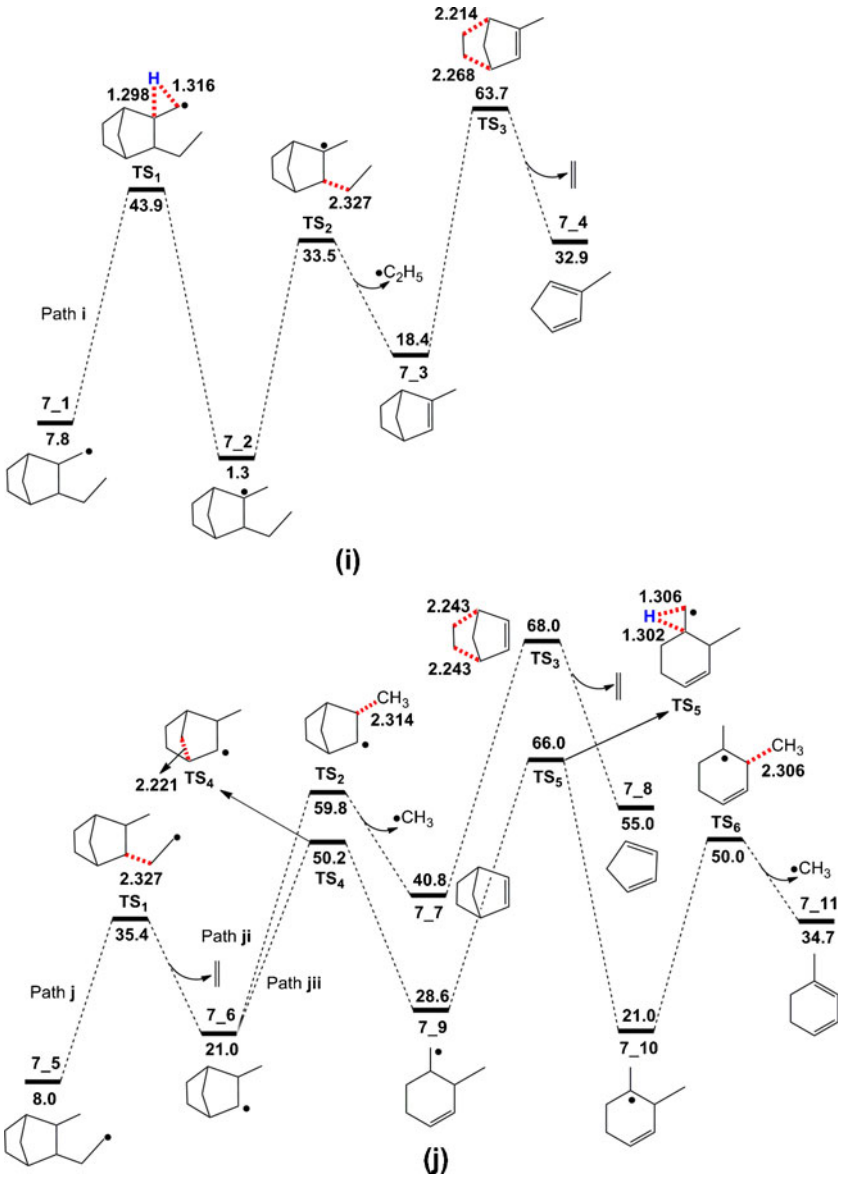

Fig. 16 The free-energy profiles for thermal cracking paths **i** and **j** (**ji**/**jii**) of diradical **R-7** of JP-10. The relative free energies are given in kcal mol^{-1}, and the bond lengths are given in angstroms (Å)

C2–C3 bond dissociates and then a hydrogen atom is transferred. Finally, the C2–C3 bond is cleaved to yield the product. The overall barrier from **3_8** to $\mathbf{TS_2}$ is calculated to be 56.1 kcal mol^{-1}. For diradical **R-4**, a hydrogen atom is transferred and then a second hydrogen atom is transferred to form **4_3**. After this, yet another hydrogen atom is transferred before the C9–C1 bond dissociates to yield 1-methylcyclopentadiene (**4_5**). The overall barrier from **4_1** to $\mathbf{TS_2}$ is calculated to be 56.5 kcal mol^{-1}. For diradical **R-5**, path **h** is energetically favorable. In path **h**, a hydrogen atom is transferred from the C4 atom to the C3 atom, which is followed by C5–C6 bond cleavage. The C7–C10 bond then breaks and a second hydrogen atom is transferred to form toluene. The overall barrier from **5_5** to $\mathbf{TS_4}$ is calculated to be 57.2 kcal mol^{-1}. For diradical **R-6**, the C3–C4 bond in **6_1** dissociates before C5–C6 bond cleavage occurs to produce ethane and radical **6_3**. The overall barrier from **6_1** to $\mathbf{TS_2}$ is predicted to be 39.0 kcal mol^{-1}. For diradical **R-7**, path **jii** is energetically favorable. In path **jii**, the C5–C6 bond in **7_5** dissociates before C7–C10 bond cleavage occurs. Then a hydrogen atom is transferred, and the subsequent C2–C3 bond cleavage yields **7_11**. The overall barrier from **7_5** to $\mathbf{TS_5}$ is calculated to be 58.0 kcal mol^{-1}. According to the calculations, path **a** of diradical **R-1** is energetically more favorable than the other possible thermal cracking paths for all of the diradicals of JP-10. The rate-determining barrier was calculated as 25.6 kcal mol^{-1}, and related to direct C6–C7 bond cleavage. The results of the calculations performed in the present work are consistent with our experimental observations that cyclopentane and cyclopentene are found in the product component analysis with high yields [29].

Conclusions

The thermal cracking pathways of JP-10 were investigated by means of density functional theory (DFT) calculations. Based on these calculations, the possible pathways for all of the diradicals obtained from the homolytic C–C bond cleavage of JP-10 were proposed. For each of these diradicals, all of the possible thermal cracking mechanisms that would yield the final products were considered. The DFT calculations showed that the products obtained from the different thermal cracking pathways are in good agreement with those seen in experimental observations. The present calculations provide new insights into the thermal cracking pathways of JP-10, and useful information for optimizing performance.

Acknowledgments The author acknowledges financial support from the National Science Foundation of China (21273201) and the China Postdoctoral Science Foundation (20110491774).

References

1. Bruno TJ, Huber ML, Laesecke A, Lemmon EW, Perkins RA (2006) NISTIR 6640
2. Striebich RC, Lawrence J (2003) J Anal Appl Pyrol 70:339–352
3. Green RJ, Anderson SL (2000) Pyrolysis chemistry of JP-10. In: Proc 13th ONR Propulsion Meeting, Minneapolis, MN, 10–12 Aug 2000
4. He KY, Androulakis IP, Ierapetritou MG (2010) Energy Fuels 24: 309–317
5. Herbinet O, Sirjean B, Bounaceur R, Fournet R, Battin-Leclerc F, Scacchi G, Marquaire PM (2006) J Phys Chem A 110:11298–11314
6. Nakra S, Green RJ, Anderson SL (2006) Combust Flame 144:662–674
7. Magoon GR, Green WH, Oluwole OO, Wong HW, Albo SE, Lewis DK (2010) A detailed JP-10 combustion mechanism constructed using RMG—an automatic reaction mechanism generator (AIAA 2010-6825). In: Proc 46th AIAA/ASME/SAE/ASEE Joint Propulsion Conf & Exhibit, Nashville, TN, USA, 25–28 July 2010
8. Davidson DF, Horning DC, Herbon JT, Hanson RK (2000) Proc Combust Inst 28:1687–1692
9. Mikolaitis DW, Segal C, Chandy A (2003) J Propul Power 19:601–606
10. Colket MB, Spadaccini LJ (2001) J Propul Power 17:315–323
11. Davidson DF, Horning DC, Oehlschlaeger MA, Hanson RK (2001) The decomposition products of JP-10 (AIAA 01-3707). In: 37th Joint Propulsion Conf, Salt Lake City, UT, USA, 8–11 July 2001
12. Xing Y, Yang X, Fang WJ, Guo YS, Lin RS (2011) Fluid Phase Equilibr 305:192–196
13. Zhang LL, Guo YS, Xiao J, Gong XJ, Fang WJ (2011) J Chem Eng Data 56:4268–4273
14. Wei H, Guo YS, Yang FJ, Fang WJ, Lin RS (2010) J Chem Eng Data 55:1049–1052
15. Yang FJ, Guo YS, Wei H, Xing Y, Fang WJ, Lin RS (2010) Chem J Chin U 31:1222–1226
16. Xie WJ, Fang WJ, Xing Y, Guo YS, Lin RS (2009) Acta Chim Sinica 67:6–12
17. Yang FJ, Guo YS, Xing Y, Li D, Fang WJ, Lin RS (2008) J Chem Eng Data 53:2237–2240
18. Xing Y, Guo YS, Li D, Fang WJ, Lin RS (2007) Energy Fuels 21: 1048–1051
19. Guo YS, Yang FJ, Xing Y, Li D, Fang WJ, Lin RS (2008) Energy Fuels 22:510–513
20. Van Devener B, Anderson SL (2006) Energy Fuels 20:1886–1894
21. Cooper M, Shepherd JE (2003) Experiments studying thermal cracking, catalytic cracking, and pre-mixed partial oxidation of JP-10 (AIAA 2003-4687). In: Proc 39th AIAA/ASME/SAE/ASEE Joint Propulsion Conf and Exhibit, Huntsville, AL, USA, 20–23 July 2003, .
22. Wohlwend K, Maurice LQ, Edwards T (2001) J Propul Power 17: 1258–1262
23. Rao RN, Kunzru D (2006) J Anal Appl Pyrol 76:154–160
24. Boyd RH, Sanwal SN, Sharyl-Tehrany S, McNally D (1971) J Phys Chem 75:1264–1271
25. Chenoweth K, van Duin ACT, Dasgupta S, Goddard WA III (2009) J Phys Chem A 113:1740–1746
26. Zehe MJ, Jaffe RL (2010) J Org Chem 75:4387–4391
27. Li SC, Varatharajan B, Williams F (2001) AIAA J 39:2351–2356
28. Hudzik JM, Asatryan R, Bozzelli JW (2010) J Phys Chem A 114: 9545–9553
29. Xing Y, Fang WJ, Xie WJ, Guo YS, Lin RS (2008) Ind Eng Chem Res 47:10034–10040
30. Zhao Y, Truhlar DG (2008) Theor Chem Acc 120:215–241

31. Zhao Y, Truhlar DG (2008) Acc Chem Res 41:157–167
32. Remya K, Suresh CH (2013) J Comput Chem 34:1341–1353
33. Liu WG, Wang SQ, Dasgupta S, Thynell ST, Goddard WA, Zybin S, Yetter RA (2013) Combust Flame 160:970–981
34. Wheeler SE (2013) Acc Chem Res 46:1029–1038
35. JanML M (2013) J Phys Chem A 117:3118–3132
36. Xu XF, Yu T, Papajak E, Truhlar DG (2012) J Phys Chem A 116: 10480–10487
37. Tishchenko O, Truhlar DG (2012) J Phys Chem Lett 3:2834–2839
38. Fukui K (1970) J Phys Chem 74:4161–4163
39. Fukui K (1981) Acc Chem Res 14:363–368
40. Gaussian 09, Revision A.1, Frisch MJ, Trucks GW, Schlegel HB, Scuseria GE, Robb MA, Cheeseman JR, Scalmani G, Barone V, Mennucci B, Petersson GA, Nakatsuji H, Caricato M, Li X, Hratchian HP, Izmaylov AF, Bloino J, Zheng G, Sonnenberg JL, Hada M, Ehara M, Toyota K, Fukuda R, Hasegawa J, Ishida M, Nakajima T, Honda Y, Kitao O, Nakai H, Vreven T, Montgomery JA, Peralta JrJE, Ogliaro F, Bearpark M, Heyd JJ, Brothers E, Kudin KN, Staroverov VN, Kobayashi R, Normand J, Raghavachari K, Rendell A, Burant JC, Iyengar SS, Tomasi J, Cossi M, Rega N, Millam JM, Klene M, Knox JE, Cross, JB, Bakken, V, Adamo C, Jaramillo J, Gomperts R, Stratmann RE, Yazyev O, Austin AJ, Cammi R, Pomelli C, Ochterski JW, Martin RL, Morokuma K, Zakrzewski VG, Voth GA, Salvador P, Dannenberg JJ, Dapprich S, Daniels AD, Farkas O, Foresman JB, Ortiz JV, Cioslowski J, Fox DJ (2009) Gaussian, Inc., Wallingford